Carbon-Efficient Conversion through Hydrogen and Formate-Driven Metabolism in *Escherichia coli*

Robert L. Bertrand*[1,2,3], Justin Panich*[2,4], Aidan E. Cowan[2,5], Jacob B. Roberts[1,2], Juliana Artier[6], Emili Toppari[1,2,7], Edward E. K. Baidoo[2,4], Yan Chen[2,4], Christopher J. Petzold[2,4], Graham A. Hudson[2,3,4], Patrick M. Shih[2,4,6,8,9], Steven W. Singer[2,4], Jay D. Keasling[1,2,3,4,10,11,A]

[1] Department of Bioengineering, University of California, Berkeley, CA, United States

[2] Joint BioEnergy Institute, 5885 Hollis St., Emeryville, CA, United States

[3] California Institute of Quantitative Biosciences, University of California, Berkeley, CA, USA

[4] Biological Systems and Engineering Division, Lawrence Berkeley National Laboratory, Berkeley, CA, United States

[5] Department of Molecular and Cellular Biology, University of California, Berkeley, CA, United States

[6] Department of Plant and Microbial Biology, University of California, Berkeley, CA, United States

[7] Department of Bacteriology, University of Wisconsin, Madison, WI, United States

[8] Environmental Genomics and Systems Biology Division, Lawrence Berkeley National Laboratory, Berkeley, CA, United States

[9] Innovative Genomics Institute, University of California, Berkeley, CA, United States

[10] Department of Chemical and Biomolecular Engineering, University of California, Berkeley, CA, United States

[11] Center for Biosustainability, Danish Technical University, Lyngby, Denmark

*These authors contributed equally to this work

[A] Corresponding author: keasling@berkeley.edu

Contributions:

RLB: Design, Experiments, Manuscript, Funding
JP: Design, Experiments, Manuscript, Funding
AEC: Experiments
JBR: Experiments
JA: Design, Funding
ET: Experiments
EEKB: Experiments
YC: Experiments
CP: Experiments
GH: Experiments
PS: Design, Manuscript, Funding
SWS: Design, Manuscript, Funding
JDK: Design, Manuscript, Funding

Key Words: Industrial microbiology | Gas fermentation | Energy Innovation | Biomanufacturing | Metabolic flux analysis | NADH | Hydrogen | Formic acid

ABSTRACT

Product yields for biomanufacturing processes are often constrained by the tight coupling of cellular energy generation and carbon metabolism in sugar-based fermentation systems. To overcome this limitation, we engineered *Escherichia coli* to utilize hydrogen gas (H_2) and formate ($HCOO^-$) as alternative sources of energy and reducing equivalents, thereby decoupling energy generation from carbon metabolism. This approach enabled precise suppression of decarboxylative oxidation during acetate growth, with 86.6 ± 1.6% of electrons from hydrogen gas (via soluble hydrogenase from *Cupriavidus necator* H16) and 98.4 ± 3.6% of electrons from formate (via formate dehydrogenase from *Pseudomonas* sp. 101) offsetting acetate oxidation. Hydrogen gas supplementation led to a titratable and stoichiometric reduction in CO_2 evolution in acetate-fed cultures. Metabolomic analysis suggests that this metabolic decoupling redirects carbon flux through the glyoxylate shunt, partially bypassing two decarboxylative steps in the TCA cycle. We demonstrated the utility of this strategy by applying it to mevalonate biosynthesis, where formate supplementation during glucose fermentation increased titers by 57.6% in our best-performing strain. Flux balance analysis further estimated that 99.0 ± 2.8% of electrons from formate were used to enhance mevalonate production. These findings highlight a broadly applicable strategy for enhancing biomanufacturing efficiency by leveraging external reducing power to optimize carbon and energy use.

GRAPHICAL ABSTRACT

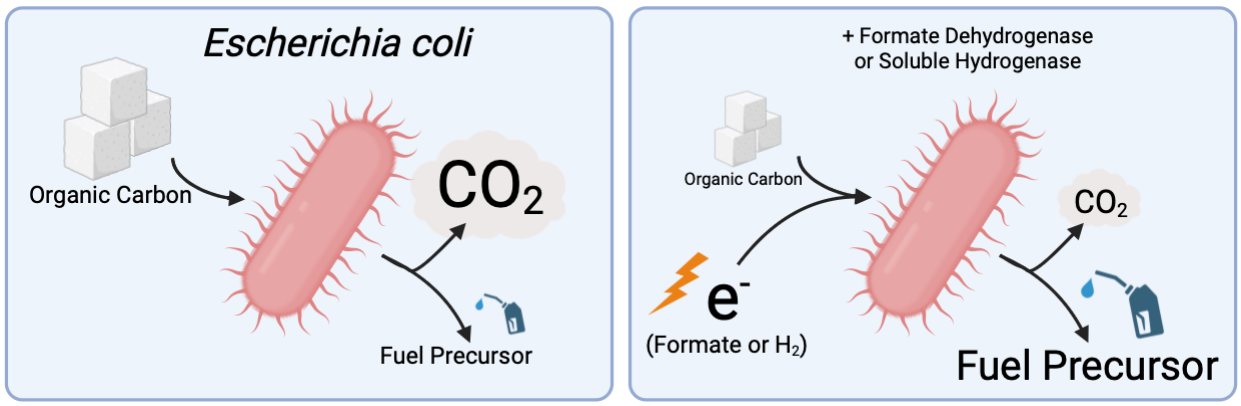

Created in BioRender. Panich, J. (2025)
https://BioRender.com/0tmtp94

INTRODUCTION

Biomanufacturing—the microbial production of chemicals and materials—provides an alternative to conventional chemical synthesis, which often depends on high temperatures, extreme pressures, and toxic catalysts[1,2]. Despite significant advances, biomanufacturing has had difficulty competing with the petroleum-based chemical industry due to higher production and feedstock costs[3,4]. Bridging this economic gap necessitates novel strategies to optimize microbial energy and carbon utilization. In heterotrophic systems, cellular energy is primarily obtained from the oxidation and decarboxylation of carbon feedstocks (e.g., glucose). The feedstock, therefore, serves a dual role as both a substrate for biosynthesis and a source of reducing power for energy generation. These mutually exclusive outcomes present a seemingly intractable problem: every molecule of feedstock oxidized to generate ATP cannot also be transformed into a desired end product[5–7]. While numerous metabolic engineering approaches[5–10] have been explored to enhance conversion and reduce carbon loss, a fundamental challenge remains: how can we meet cellular energy demands without compromising product yield? Addressing this bottleneck is critical if industrial microbiology is to become economically competitive.

The advent of electrolysis technology and the increasing availability of inexpensive electricity enable the consideration of biomanufacturing platforms that provide cells with external sources of reducing power. When energy is abundant, cells downregulate feedstock oxidation through catabolic pathways[14–16]. Therefore, supplying an external source of reducing power should free feedstock from its traditional role as cellular fuel, bypassing this problem altogether. This can be accomplished by equipping common industrial hosts with a mechanism for indirect electron transfer through electron carriers such as formate ($HCOO^-$) or hydrogen gas (H_2)[11,12]. Formate is readily oxidized by NAD^+- or $NADP^+$-specific formate dehydrogenase (FDH) to regenerate NADH or NADPH, and numerous structurally distinct FDH homologs are available to meet various performance criteria (catalytic efficiency, thermostability, proteolytic resistance, etc.). Formate is highly soluble, membrane-permeable, and can be electrochemically produced from CO_2. However, it is toxic at high concentrations and requires pH buffering[13,14]. NADH could be regenerated by oxidizing H_2 via hydrogenases. The sole byproduct of this reaction is a proton, which becomes covalently bound once NAD(P)H is re-oxidized (such as in respiration), thereby providing total atom economy and pH neutrality. Furthermore, H_2 is non-toxic and energy-dense by unit mass. However, H_2 is energy sparse by unit volume, poorly soluble in water, and explosive when mixed with oxygen (between 5-85% H_2).

To investigate the effects of adding external reducing equivalents on metabolism, we have engineered *E. coli* to express the O_2-tolerant soluble hydrogenase (HYD) from the chemolithoautotrophic microorganism *Cupriavidus necator* H16. In parallel experiments, we also used the FDH from *Pseudomonas sp. 101*. Both strains showed decreased feedstock consumption and increased product titer (mevalonate), indicating a broad potential for biomanufacturing.

MATERIALS AND METHODS

DNA Manipulations: Routine PCR was performed using Phusion Polymerase Hot Start II (*ThermoFisher*, Waltham, MA, USA) under the following conditions: 1 minute at 94°C; 25 cycles of 10 seconds at 94°C, 15 seconds at T_m - 4°C, and 20 seconds per kb at 72°C; followed by an additional 20 seconds per kb at 72°C. Amplicons were resolved by agarose gel electrophoresis, evaluated using gel imaging (*Bio-Techne*, Minneapolis, MN, USA), and purified with the QIAquick gel extraction kit (*Qiagen*, Hilden, Germany). Plasmid construction was carried out either by Gibson assembly with the NEBuilder HiFi DNA Assembly Master Mix *(New England Biolabs*, Ipswich, MA, USA) or through ligation using T4 DNA Ligase (*ThermoFisher*, Waltham, MA, USA). Candidate constructs were cloned using chemically competent "Stellar" *E. coli* (*Takaro Bio*, San Jose, CA, USA), and then authenticated either by nanopore sequencing (*Plasmidsaurus*, San Francisco, CA, USA) or by Sanger sequencing (*Azenta*, Burlington, MA, USA). Verified plasmids were subsequently transformed into DE3-competent BW25113 *E. coli* via electroporation. Plasmids (Table S1), primers (Table S2), bacterial strains (Table S3), and the plasmid assembly scheme (Figure S1) are available in the SI.

Growth Media and Conditions: Hydrogenase prototyping experiments were conducted using Miller LB medium (*Millipore*, Burlington, MA, USA) and sterilized by autoclaving (hereafter "LB"). Acetate consumption assays utilized a rich media solution of MOPS, amino acids, and nucleotides (EZ Rich Defined Medium Kit: *Teknova*, Hollister, CA, USA), containing 55.5 mM sodium acetate, and was sterilized by 0.2-µm membrane filtration (hereafter "EZ Acetate"). Adding 5 g/L glucose instead of acetate produces "EZ Glucose." Mevalonate production assays were carried out using M9 minimal medium containing 5 g/L glucose, 0.12 g/L $MgSO_4$, 0.011 g/L $CaCl_2$, 65 µg/L $NiCl_2$, and a trace elements mixture containing (100x) 5 g/L EDTA, 0.83 g/L $FeCl_3$-$6H_2O$, 84 mg/L mM $ZnCl_2$, 13 mg/L $CuCl_2$-$2H_2O$, 10 mg/L $CoCl_2$-$2H_2O$, 10 mg/L H_3BO_3, and 1.6 mg/L $MnCl_2BO_3$-$4H_2O$. This medium was sterilized by 0.2 µm membrane filtration (hereafter "M9 Glucose"). A bacterial washing step was performed using the same M9 minimal medium, but with glucose omitted (hereafter "M9 Wash").

Gas Cultivations: Glycerol stocks of BW25113 and CM15 *E. coli* were plated on LB agar with the appropriate antibiotics (*Teknova*, Hollister, CA, USA). Colonies were seeded into 10 mL of either LB, EZ Acetate, or M9 Glucose, and grown aerobically in culture tubes overnight at 37°C and 200 RPM for <18 h. Experimental cultures were established by inoculating 200 µL of seed cultures into 10 ml of the same medium (LB, EZ Acetate, or M9 Glucose) in glass serum bottles. Cultures were grown mid-logarithmically by aerobic cultivation at 37°C and 150 RPM for 4 h. The cultures were then transferred to a 30°C warm room. Hydrogenase expression was induced using 0.25 mM IPTG, whereas formate dehydrogenase expression was constitutively expressed. Bottles were closed with butyl stoppers and crimped with aluminum to create an airtight seal. From the approximately 112 mL headspace, 20 mL of atmospheric air was removed using a syringe fitted with a one-way stop valve. The cultures expressing hydrogenase were then supplied with either 20 mL of H_2 gas (800 µmol) or 20 mL of N_2 gas. The H_2 addition step is accurate to ± 5 µmol H_2 (Table S4 in *SI*). The cultures expressing formate dehydrogenase were given either 40 mM sodium formate or a water blank and otherwise equivalently treated by withdrawing 20 mL of

air, followed by adding 20 mL of N_2 gas. Cultures were grown for 18 h at 150 RPM and 30°C. To enhance H_2 uptake during mevalonate assays when *E. coli* was cultivated in glucose minimal medium, a variant procedure was performed as follows: Seed cultures were inoculated (200 µL) into 10 mL of EZ Glucose in glass serum vials and grown aerobically at 37°C and 150 RPM for 4 h. Cultures were then transferred to a 30°C warm room, induced with 0.25 mM IPTG, and allowed to grow aerobically for four more hours. Cells were centrifuged and resuspended in M9 Wash. Cells were again centrifuged and then resuspended in M9 glucose (5 g/L) containing 0.25 mM IPTG. Serum vials were stoppered and crimped, and 20 mL of air was replaced with 20 mL of H_2 or N_2. Cultures were incubated for 18 h at 150 RPM and 30°C. Culture density was evaluated using optical density (OD_{600}) and/or dry cell weight (g/L). The DCW was measured by concentrating an aliquot of bacterial suspension within pre-weighed microcentrifuge tubes, followed by drying for 48 hours. The consensus OD600/DCW ratio was 3.07 ± 0.17, in agreement with prior studies[15]. The DCW was measured in most experiments, and actual DCW readings are shown in figures wherever possible. In cases where only OD_{600} data were collected, these readings are converted into DCW using the consensus ratio, as indicated in figure captions. Diagrams of key experimental schemes are provided (Figures S2 to S4 in the *SI*). Statistical replicate cultures of BW-HYD grown in EZ-Acetate revealed statistical variations of 1% to 4% with respect to OD_{600}, dry cell weight (DCW), CO_2 production, and broth acetate concentration (Table S5 in *SI*).

Gas Analysis: The GoDirect Gas Pressure Sensor (*Vernier*, Beaverton, OR, USA) was used to monitor the internal gas pressure of serum bottles. Broth aliquots for downstream analyses (e.g., HPLC) were collected either using a needle and syringe or by opening serum vials with needle-nose pliers and removing aliquots by pipetting. Accurate CO_2 quantification was achieved by gasifying dissolved CO_2 through the acidification of the media with a few drops of concentrated HCl. Gas analysis was conducted using a Shimadzu GC-2014 gas chromatograph, withdrawing gas aliquots from butyl-stoppered serum vials with syringes fitted with one-way stop valves. Samples flowed isothermally through a 2 mm x 8 m Shimadzu (Kyoto, Japan) column at 60°C using argon as the carrier gas. H_2, O_2, and N_2 were quantified after 8.5 minutes of flow time through a TCD module at 120°C, with CO_2 quantified after an additional 4.0 minutes of flow time through the methanizer at 380°C and FID module at 200°C. The gas profile was quantified by interpolating peak integrations to standard plots, using inert N_2 as an internal standard. Gasses are quantifiable by GC with an error of ± 0.21% (Table S6 in SI).

***In Vitro* Hydrogenase Assays:** Cells were inoculated from an overnight pre-culture in LB with appropriate antibiotics and induced for hydrogenase expression at 30°C during the mid-log phase. Cells were cultivated for 24 or 48 h, cold centrifuged, and lysed by sonication. Total protein content was evaluated using the Bradford assay. Hydrogenase activity from lysates was assessed with an NADH absorption assay at 340 nm, as previously described[16]. This work was performed in an anaerobic growth chamber containing 4% H_2 and 10% CO_2, and assays were analyzed using a 340PC SpectraMax spectrophotometer (*Molecular Devices,* San Jose, CA, USA).

Extracellular Metabolite Quantification: The profiles of extracellular metabolites were evaluated using HPLC. Samples were prepared by isolating the broth supernatant and adding

10% methanol to create an internal loading standard. The samples were filtered through 0.45-µm modified nylon centrifugal filters (*VWR*, Radnor, PA, USA), and the filtrates were stored at -80°C until needed. The samples were analyzed isothermally on an Aminex HPX-87H column (*BioRad*, Hercules, CA, USA) set to 65°C, with a refractive index detector set to 50°C (*Agilent*), and the sample loading tray maintained at 8°C (*Agilent*, Santa Clara, CA, USA). The mobile phase consisted of 0.005 M H_2SO_4 and flowed at a rate of 0.6 ml/min. Data acquisition and analysis were performed using ChemStation software (*Agilent*, Santa Clara, CA, USA). The broth concentrations of glucose, formate, ethanol, acetate, glycerol, lactate, succinate, and mevalonate were quantified by interpolating peak integrations against authenticated standards (*Sigma-Aldrich*, St. Louis, MO, USA). Acetate is quantifiable by HPLC with an error margin of ± 2.2 µmol (Table S7 in *SI*).

Additional Materials and Methods: Methods for LC-MS, protein identification and quantification, HPLC-MS, computational flux balance analysis, and deductive metabolic estimations are found in the *SI*.

RESULTS AND DISCUSSION

Prototyping the *C. necator* soluble hydrogenase (HYD) and *Pseudomonas sp.* 101 formate dehydrogenase (FDH): NAD^+-dependent hydrogenases reversibly reduce the nicotinamide cofactor with electrons from H_2[17]. While most hydrogenases are sensitive to O_2 and are inactivated upon contact with air[18], a key exception is the soluble and O_2-tolerant hydrogenase from *C. necator* H16 (formerly *Ralstonia eutropha* H16)[19], an organism that has drawn attention for its ability to use energy gained from H_2 to aerobically fix CO_2 and transform it into bioplastics and biofuels[20,21]. The soluble hydrogenase is a heterotetramer (HoxFUYH), and its heterometallic NiFe catalytic core and iron-sulfur clusters require nine maturation proteins (HoxWI and HypABCDEFX) to assemble.

The heterologous expression of 13 soluble proteins in a heterologous host presents a considerable challenge. However, it has already been functionally expressed in *E. coli,* providing a catalog of genetic components[22–2627]. The existing expression constructs were non-optimal due to missing genes, non-codon-optimized genes, and multiple plasmids. Using the genetic components described in Lamont and Sargent (2017)[26], we consolidated all 13 genes into a single plasmid containing the medium copy p15A origin of replication and kanamycin resistance, organized into two operons (T5 and *tatA* promoters) (Figure S1 in *SI* for assembly scheme and Figure S5 in *SI* for plasmid map). Transforming this plasmid into *E. coli* BW25113 resulted in strain BW-HYD. Cultivating this strain with H_2 in sealed bottles demonstrated hydrogenase's functional activity, directly by gas chromatography (Figure 1A) and evidenced indirectly by pressure monitoring (Figure 1B). We complemented these experiments with metabolomics analyses to investigate any effects that H_2 may have on BW-HYD metabolism. In line with literature[44], cultures treated with H_2 displayed increased cellular concentrations of reduced metabolites of the TCA cycle (succinate, fumarate, malate) compared to N_2-treated controls (Figure S6). We hypothesize that cells respond to H_2 uptake by engaging the glyoxylate shunt, a carbon-conserving bypass of the TCA cycle that reduces carbon loss as CO_2 by minimizing

decarboxylative NADH generation[28]. This hypothesis is supported by biosynthetic studies utilizing the glyoxylate shunt to enhance the production of succinate, fumarate, malate, and other closely related intermediates[29].

We then conducted biochemical characterization experiments to compare the specific activity of our construct in *E. coli with* lysates from autotrophically grown *C. necator* H16. Cells were grown for the indicated times, lysed, and monitored for NADH formation in saturating NAD^{+}[16]. The resultant hydrogenase activity observed from BW-HYD was comparable to the activity measured in *C. necator* (942 U/g DCW and 1310 U/g DCW, respectively, which is consistent with previous reports for soluble hydrogenase activity in *C. necator* H16[30]) (Figure 1C). In addition, we performed quantitative proteomics on the 13 heterologous proteins expressed in *E. coli* and compared these results with those from autotrophically grown *C. necator*. We observed that the expression of HoxY in *E. coli* is substantially lower than that of HoxFUH, indicating an unbalanced expression of the heterotetramer (Figure 1D). Moreover, BW-HYD produced many maturation proteins at higher levels than those in *C. necator*, suggesting that maturation proteins are expressed in excess. Cumulatively, these experiments demonstrate that a prototype plasmid encoding the C. necator hydrogenase and its maturation machinery was successfully constructed and functionally expressed in *E. coli*, but that expression stoichiometry should be considered during future optimization efforts, as more cellular energy appears to be expended assembling proteins than is minimally required.

To broaden the scope of this study, we employed a formate dehydrogenase (FDH) as an alternative mechanism for assimilating external electrons. We selected the FDH from *Pseudomonas sp.* 101, which has been extensively characterized in *E. coli*[31–33]. Transforming a plasmid encoding this FDH into *E. coli* BW25113 yielded strain BW-FDH. In cell lysates, this FDH exhibited over a fourfold increase in specific activity for NADH formation compared to HYD (Figure 1C). The superior performance of FDH could relate to its simpler expression and maturation requirements compared to hydrogenases.

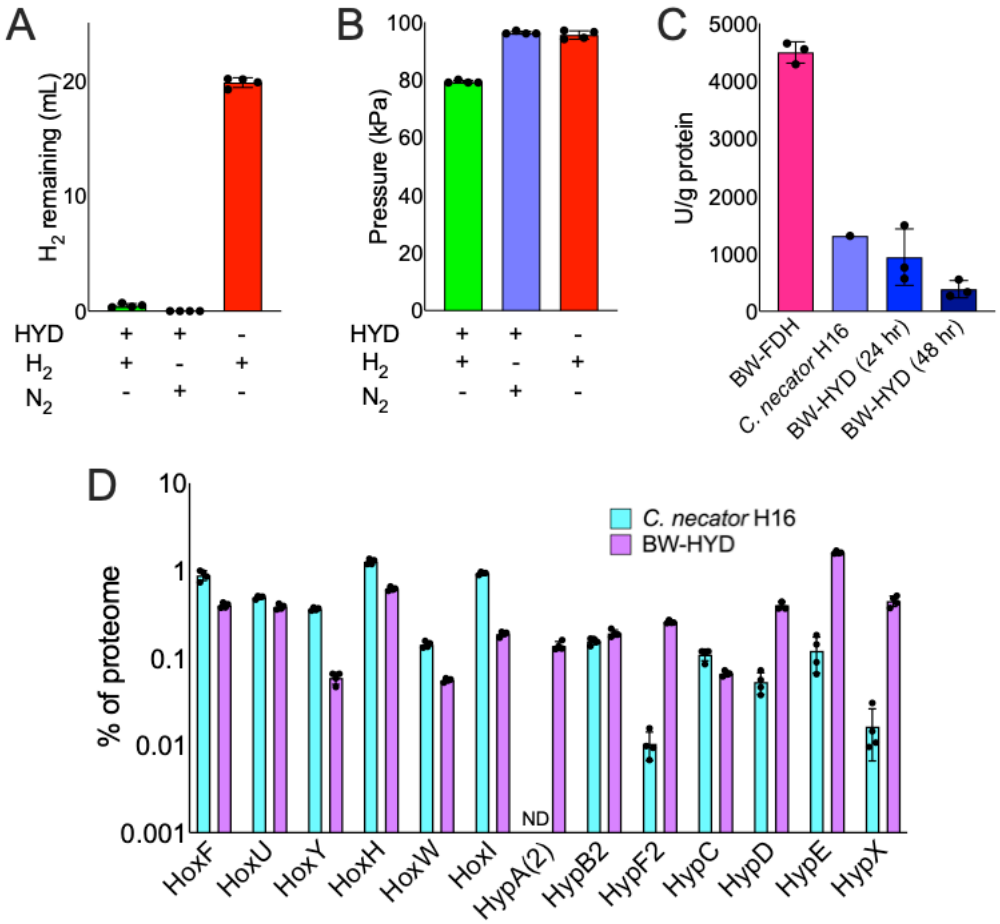

Figure 1: Characterizing the heterologous soluble hydrogenase from *C. necator* H16 in *E. coli*. (A) H_2 consumption (expressed as ml H_2 remaining in headspace) by *E. coli* BW25113 expressing *C. necator* hydrogenase (BW-HYD), when initially provided with 20 ml H_2 mixed with air, compared to the same strain provided with 20 ml N_2 mixed with air, and untransformed BW25113 fed with 20 ml H_2 mixed with air, after an overnight incubation in sealed serum bottles containing approximately 112 ml headspace. **(B)** Final internal pressure of enclosed serum vials of these same cultures. **(C)** Specific *in vitro* activity measurements of *C. necator* hydrogenase within crude lysates of BW-HYD after 24h or 48h of cultivation (n=3), compared to this same hydrogenase when expressed within the native producer (*C. necator* H16) grown in 62% H_2 / 10% CO_2 / 10% O_2, balanced with N_2 (n=1). The specific activity of the *Pseudomonas sp.* FDH on formate was used as a reference control when grown for 24 h[33] (n=3). **(D)** Proteomics analysis to quantify the protein abundance of the 13 *C. necator* hydrogenase heterotetramer and maturation proteins when expressed in *E. coli*, in comparison to their natural expression levels in *C. necator* (n=4). HypA is denoted HypA(2) because HypA1 and HypA2 sequences are identical; ND = Not detected. See Figure S5 in the *SI* for the plasmid map.

Electron donors prevent the decarboxylation of an organic carbon feedstock. The oxidation of H_2 and $HCOO^-$ results in the regeneration of NADH. Either donor should satisfy cellular energy requirements because NADH can drive oxidative phosphorylation or transfer its hydride equivalent to regenerate NADPH through the native transhydrogenase PntAB. We tested both donors' ability to inhibit the oxidative decarboxylation of feedstock by cultivating BW-HYD on acetate. Acetate was chosen because NADH production from this feedstock depends solely on the TCA cycle, which simplifies experimental interpretation[31]. The defined rich medium also contained amino acids and nucleotides as secondary carbon sources.

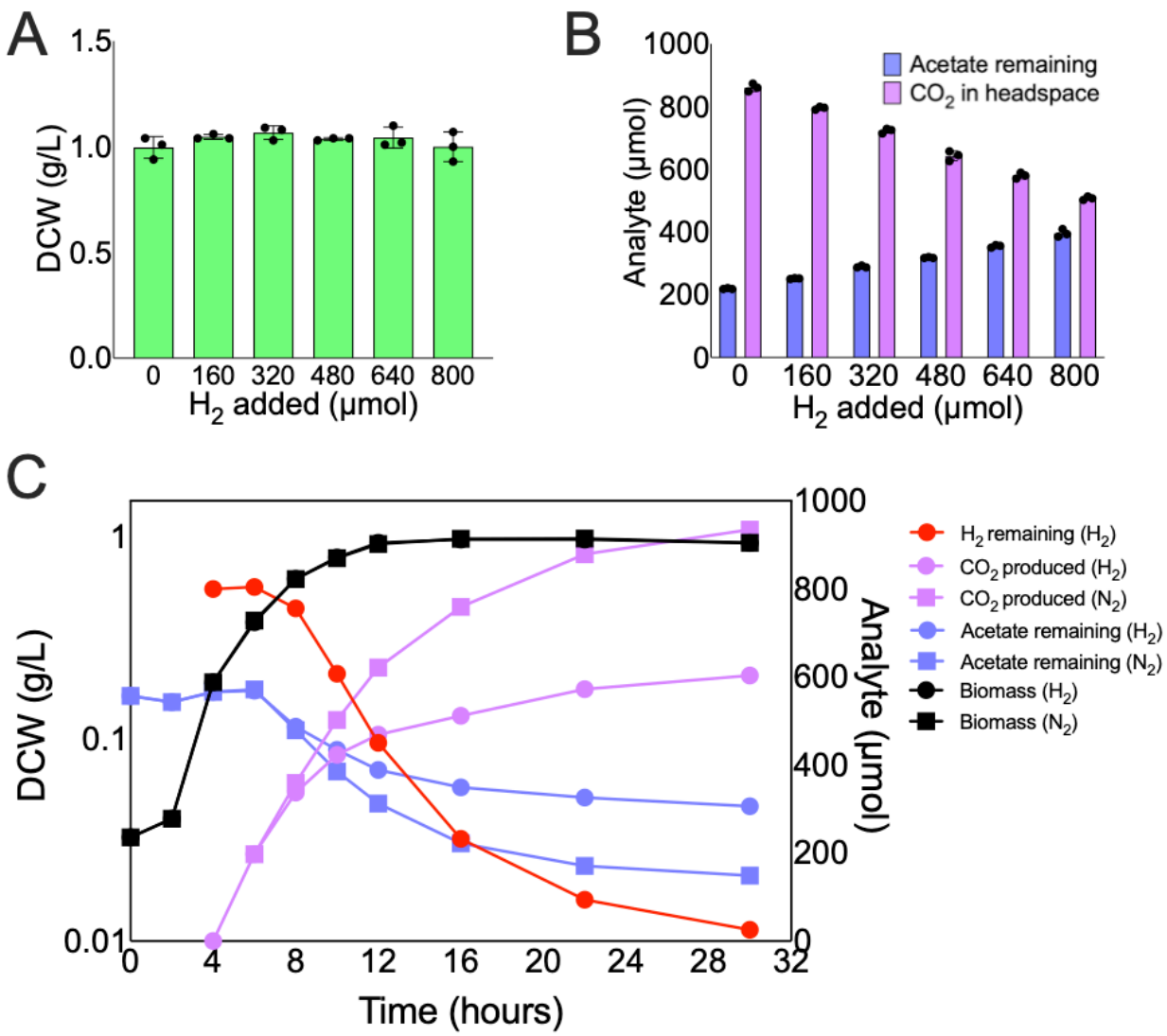

Figure 2: Titrating the metabolic effects of H_2 uptake on acetate consumption and CO_2 production in BW-HYD. (A) Biomass formation (dry cell weight) after an overnight incubation (n=3). Hydrogen gas uptake data are shown in Figure S7 in the *SI*. **(B)** Acetate remaining in the culture media (µmol) and carbon dioxide produced (µmol) (n=3). Plots of H_2 expended versus acetate retained, and of CO_2 avoided versus acetate retained, are available in Figure S8 in the *SI*. **(C)** A time course experiment evaluating the effects of H_2 uptake on acetate retention and CO_2 production by BW-HYD, compared to the same strain subjected to an inert N_2 treatment. Either 20 ml of H_2 (800 µmol) or 20 ml of N_2 was added to the headspace of each culture at time = 4 hours. Biomass accumulation is shown in black, measurements of H_2 are shown in red, acetate measurements in solution are shown in blue, and CO_2 measurements are shown in purple. Circles represent cultures incubated in air and fed with H_2, while squares represent cultures incubated in air and treated with an equivalent volume of inert N_2. The culture optical density (OD_{600}) was recorded and converted into DCW using the consensus ratio (see *Gas Cultivations*). The experiment was performed in technical triplicate using a common seed culture inoculum (n=3). Error bars are occluded by symbols.

BW-HYD was cultivated in a rich defined medium containing 55.5 mM acetate as the primary carbon source (see experimental scheme in Figure S2A). Mid-logarithmic phase cultures were provided with increasing amounts of H_2 (0 to 800 µmol). After an overnight (16h) incubation in butyl-stoppered serum vials, the effects of H_2 uptake on biomass formation, acetate retention, and CO_2 production were evaluated. Results show that all cultures consumed most (>80%) of the H_2

supplied (Figure S7 in *SI*) and that H_2 consumption did not alter how much biomass formed, thereby normalizing this variable (Figure 2A). A linear molar relationship between H_2 uptake and acetate retention was observed (3.925 ± 0.062; Figure S8B in *SI*), demonstrating that BW-HYD consumed less acetate to produce the same amount of biomass. This improved efficiency coincided with a decrease in CO_2, indicating that less feedstock was oxidized (Figure 2B). According to stoichiometry, in order to prevent the formation of two moles of CO_2, it is necessary to also reduce the oxidation of one mole of acetate. This stoichiometry was observed (2.035 ± 0.036; Figure S8A in *SI*), providing direct evidence that the oxidation of hydrogen gas was replacing the oxidation of acetate as a means of generating cellular energy.

Feedstock preservation was also demonstrated through a time-course assay. H_2 uptake, biomass formation, and acetate consumption were evaluated over 30 hours, during which cultures of BW-HYD were grown in 55.5 mM acetate, supplied with either 20% H_2 in air or 20% N_2 in air, and harvested at specified times (see experimental scheme in Figure S3 in *SI*). Changes in H_2 uptake, CO_2 production, and acetate consumption appeared four hours after IPTG induction, indicating that *E. coli* required approximately four hours to translate and activate the hydrogenase (Figure 2C). The peak H_2 consumption rate was 5.4 mmol H_2 / g_{DCW} / h. Acetate concentration decreased at 8 h, coinciding with the onset of H_2 uptake at this time and changes in CO_2 production, suggesting a causal relationship. Although the observed accumulation of biomass without acetate consumption during the first six hours might indicate sequential substrate utilization of amino acids and nucleotides within the rich media, we could not resolve distinct biphasic growth kinetics typically indicative of diauxic growth (Figure 2C).

While H_2 is attractive for its low cost and energy density, formate is a non-explosive energy carrier that can similarly power microbial metabolism and may have broader utility. To this end, we performed an equivalent end-point titration using sodium formate (see experimental scheme in Figure S2B in *SI*). Formate can be oxidized by FDH into NADH and CO_2 using the BW-FDH strain, which was cultivated similarly to BW-HYD. In triplicate cultures, increasing amounts of formate (0 to 400 μmol) were fed to BW-FDH during the mid-logarithmic phase. Cultivation in butyl-stoppered serum vials enabled CO_2 measurements. Following the experiment, formate was undetectable, suggesting that 100% of the formate was consumed under all tested conditions (Figure S9A in *SI*). As observed with BW-HYD grown with H_2, biomass formation was unaffected by formate addition, normalizing cellular energy requirements among triplicates (Figure 3A). A titratable molar relationship (2.865 ± 0.103; Figure S8D in *SI*) emerged between formate addition and acetate retention. The oxidation of formate produces CO_2 as a byproduct, which complicates our assessment of the relationship between CO_2 emissions and acetate oxidation (Figure S9B in *SI*). Therefore, to determine moles of biogenic CO_2, we subtracted moles of formate oxidized from the total amount of CO_2 observed in the headspace (Figure 3B). A stoichiometric relationship (1.933 ± 0.110; Figure S8C in *SI*) was revealed between biogenic CO_2 abatement and acetate preservation, demonstrating that this alternative electron donor is also capable of suppressing the oxidation of a feedstock.

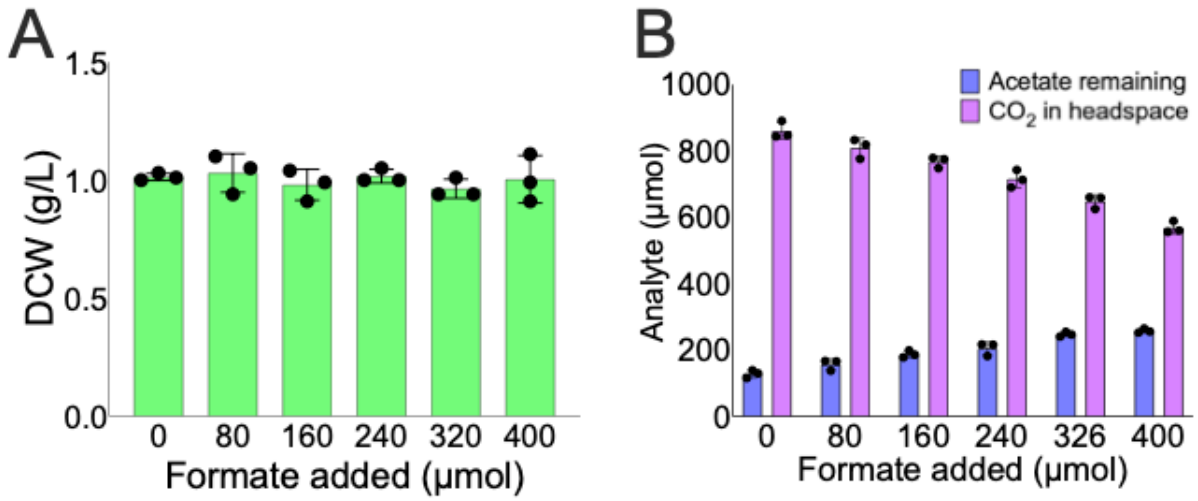

Figure 3: Titrating the metabolic effects of formate uptake on acetate retention and CO_2 production in BW-FDH. (A) Biomass formation at the end of an overnight incubation (dry cell weight) (n=3). These data show that formate uptake did not influence the amount of biomass formed, thereby normalizing biomass as a variable when examining the effects of formate uptake on acetate consumption and CO_2 production. Formate uptake data are presented in Figure S9 in the *SI*. **(B)** Acetate remaining in the culture media and biogenic CO_2 produced (n=3). Biogenic CO_2 is calculated by subtracting the moles of formate oxidized from total CO_2 (μmol). Total CO_2 production can be found in Figure S9B in the *SI*.

Electron donors increase mevalonate yield with optimizable efficiency: Our results thus far demonstrate that electron donors can supplant an organic feedstock as the source of cellular energy needed to generate biomass. We next explored whether feeding H_2 and $HCOO^-$ to *E. coli* could enhance the production of a single target bioproduct. We selected mevalonate (MEV), a central metabolic intermediate in isoprenoid biosynthesis with broad utility as a precursor to numerous high-value bioproducts. To investigate, we inserted plasmids encoding hydrogenase, formate dehydrogenase, and genes for mevalonate biosynthesis (Table S1 in *SI*), yielding strains BW-HYD-MEV and BW-FDH-MEV (Table S3 in *SI*). Preliminary experiments using the same acetate-based rich medium as in the preceding section revealed a baseline mevalonate titer of only 30 mg/L (Figure S10 in *SI*), a low value[34] that limits our ability to clearly resolve differences in titer between experimental conditions. The low mevalonate titer was likely observed because acetyl-CoA is required for MEV biosynthesis, and it is well established that acetyl-CoA is limited in cells grown on acetate due to competing demands from central carbon metabolism and enzymatic bottlenecks such as acetyl-CoA carboxylase[35]. In contrast, glucose is commonly used in industry to make commodity chemicals, including MEV, and we observed that growing BW-HYD-MEV and BW-FDH-MEV in glucose (5 g/L) minimal media routinely achieved baseline MEV titers between ~0.5 and 1.0 g/L (Figure 4). However, we also observed that H_2 consumption by BW-HYD was negligible when we applied the same cultivation protocol used in the preceding section, which involved the induction of hydrogenase and introduction of H_2 at 4h post-inoculation (Figure S2A in *SI*). We anticipated that the cultivation protocol would need to be adjusted because H_2 uptake by exogenous hydrogenases is variable due to genetic background and cultivation conditions[25,35]. The results shown in Figure 2C provided two clues for protocol development: (1) hydrogenases require 4h to mature following IPTG induction, and (2) robust hydrogenase

395 expression is apparent in rich media. We tested a modified protocol wherein BW-HYD was first
396 inoculated into rich medium and grown for 4h to mid-logarithmic phase. Hydrogenase expression
397 was induced with IPTG, and cells were grown for an additional 4h. The cells were then washed,
398 transferred to glucose minimal medium, and cultivated overnight in defined headspaces
399 composed of 20% H_2 in air or 20% N_2 in air (control condition) (Figure S4B in *SI*). This protocol
400 resulted in BW-HYD consuming about 15 of the 20 mL of H_2 provided, a promising result for its
401 subsequent application on BW-HYD-MEV (Figure S11 in *SI*). In contrast to hydrogenase, no
402 formate uptake obstacles were observed when *E. coli* was grown in glucose minimal medium.
403 Therefore, a simpler 4h post-inoculation protocol was used for BW-FDH-MEV (Figure S4B in *SI*).

404 The results of these parallel experiments are shown in Figure 4. BW-HYD-MEV utilized 181 μmol
405 of the 800 μmol H_2 in headspace (Figure 4A). Despite this limited uptake, there was a modest
406 increase in MEV titer from 18.0 ± 0.5 to 20.2 ± 0.8 μmol (0.266 to 0.299 g/L) (Figure 4B). These
407 data suggest that 82.3 moles of H_2 were oxidized for each mole of surplus MEV produced.
408 Although minimal differences in biomass formation were noted (Figure 4C), H_2 prompted the
409 production of C_1 (formate) and C_2 (ethanol and acetate) mixed acid products (Figure 4D; Table
410 S8 in *SI*). Compared to BW-HYD-MEV, all 400 μmol of formate supplied to BW-FDH-MEV were
411 fully consumed, as shown by the absence of detectable formate in the culture supernatant after
412 overnight cultivation (Figure 4F). This formate elevated mevalonate production from a baseline
413 titer of 49.1 ± 2.1 to 59.3 ± 1.2 μmol (0.73 to 0.88 g/L) (Figure 4G), providing a ratio of 39.2 moles
414 of formate oxidized per mole of surplus MEV generated. Sample readings revealed that the
415 addition of formate also enhanced the production of biomass (Figure 4H) and mixed acids (Figure
416 4I). These experiments demonstrate that both electron donors can boost the production of a
417 commodity chemical, but much of the extra reducing power was redirected to generate surplus
418 biomass and mixed acids.

419 We hypothesized that blocking pathways responsible for mixed acid production would redirect
420 carbon flux toward mevalonate synthesis, thereby enhancing its production. We tested this
421 hypothesis using *E. coli* CM15 (MG1655 *ΔaraBAD ΔfadRE ΔldhA ΔackApta ΔadhE ΔpoxB*
422 *ΔfrdABCD*)[36], establishing equivalent strains CM-HYD-MEV and CM-FDH-MEV by introducing
423 the appropriate plasmids (Table S3 in *SI*). Hydrogen gas uptake by CM-HYD-MEV was modest
424 at only 70 μmol H_2 (Figure 4A) but increased the baseline MEV titer from 20.0 ± 0.5 to 21.7 ± 0.5
425 μmol (0.296 to 0.322 g/L) (Figure 4B). This provides an H_2/MEV molar ratio of only 41.2, a two-
426 fold improvement compared to the ratio of 82.3 obtained with BW-HYD-MEV. The consumption
427 of 400 μmol of formate by CM-FDH-MEV (Figure 4F) substantially improved the baseline titer
428 from 52.9 ± 0.1 to 83.3 ± 0.8 μmol (0.78 to 1.23 g/L) (Figure 4G). This signifies a three-fold
429 improvement in the formate/mevalonate molar ratio from 39.2 (BW-FDH-MEV) to only 13.2.
430 Notably, using CM15 minimized differences in biomass and mixed acid formation (Figure 4C, 4D,
431 4H, 4I), demonstrating that fewer electrons from these electron donors were used to enhance off-
432 target effects. These experiments show that electron donors can promote the formation of a
433 commodity chemical and that donor utilization efficiency can be improved by metabolically
434 remodeling the host strain.

435

436

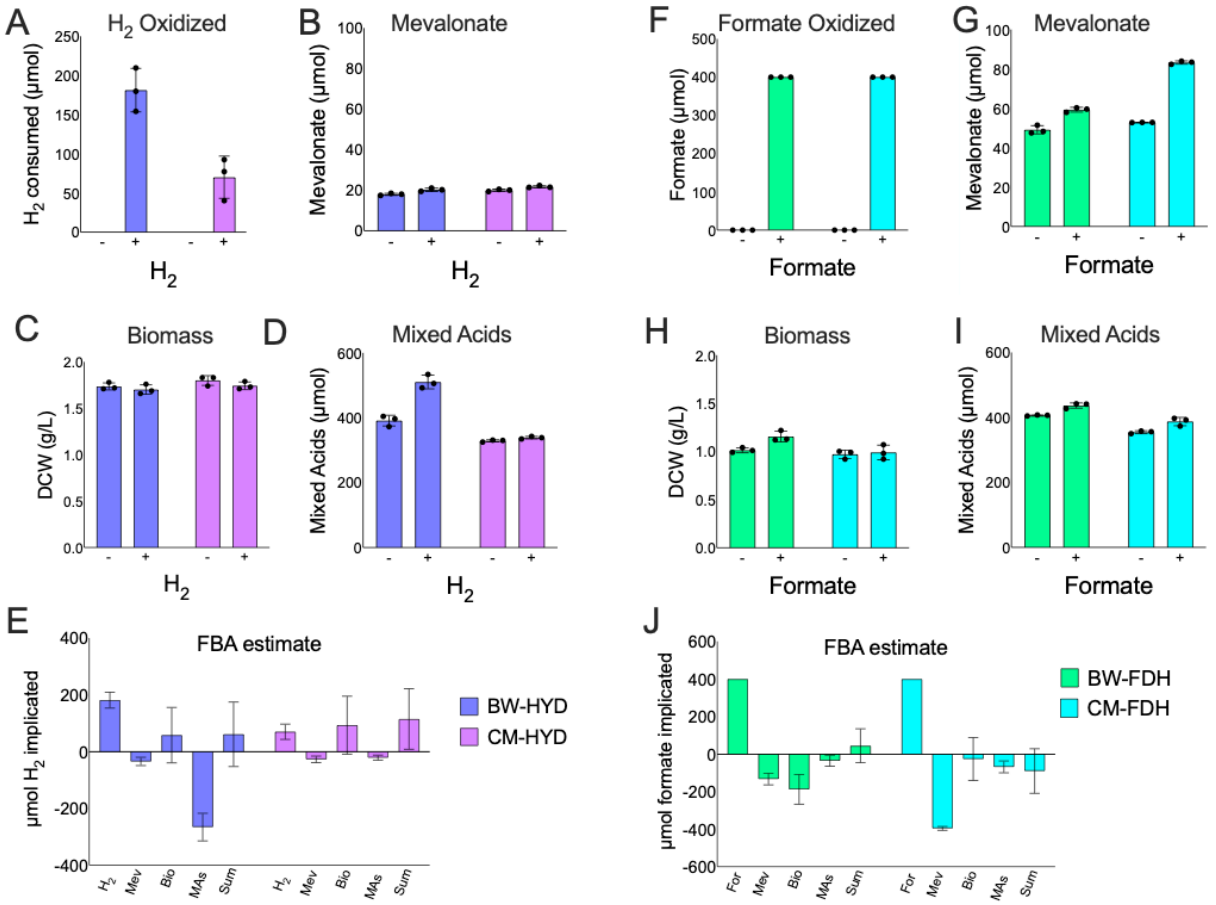

Figure 4: Effects of hydrogen gas (A-E) and formate (F-J) on the biochemical profiles of BW-FDH-MEV (blue/purple bars) and CM-FDH-MEV (green/cyan bars) in glucose M9 minimal media. (A, F) Amounts of formate and hydrogen gas consumed (µmol). **(B, G)** Mevalonate produced (µmol). **(C, H)** Dry cell weight (g/L). **(D, I)** Profile of mixed acid production (µmol), summed by the moles of carbon atoms contained within formate, ethanol, acetate, glycerol, lactate, and succinate; micromoles of each mixed acid are detailed in Table S8 in *SI*. **(E, J)** Estimates from computational flux balance analysis (FBA) of the hydrogen gas or formate required to produce each biochemical difference observed between electron-treated and blank-treated cultures, where negative values indicate the amount of hydrogen gas or formate that must be theoretically oxidized to produce that change, and positive values suggest either the donation of electrons or its equivalence in surplus cellular energy. Only acetate, ethanol, and formate (in hydrogenase-laden cultures) were analyzed for fermentation impact since these three molecules made up >95% of the mixed acid profile. The sum of positive and negative contributors is expected to fall within the margin of zero micromoles, as discussed in *the flux balance analysis to evaluate the efficiency of hydrogen gas and formate usage*. Abbreviations: Mev = Mevalonate; Bio = Biomass; MAs = mixed acids.

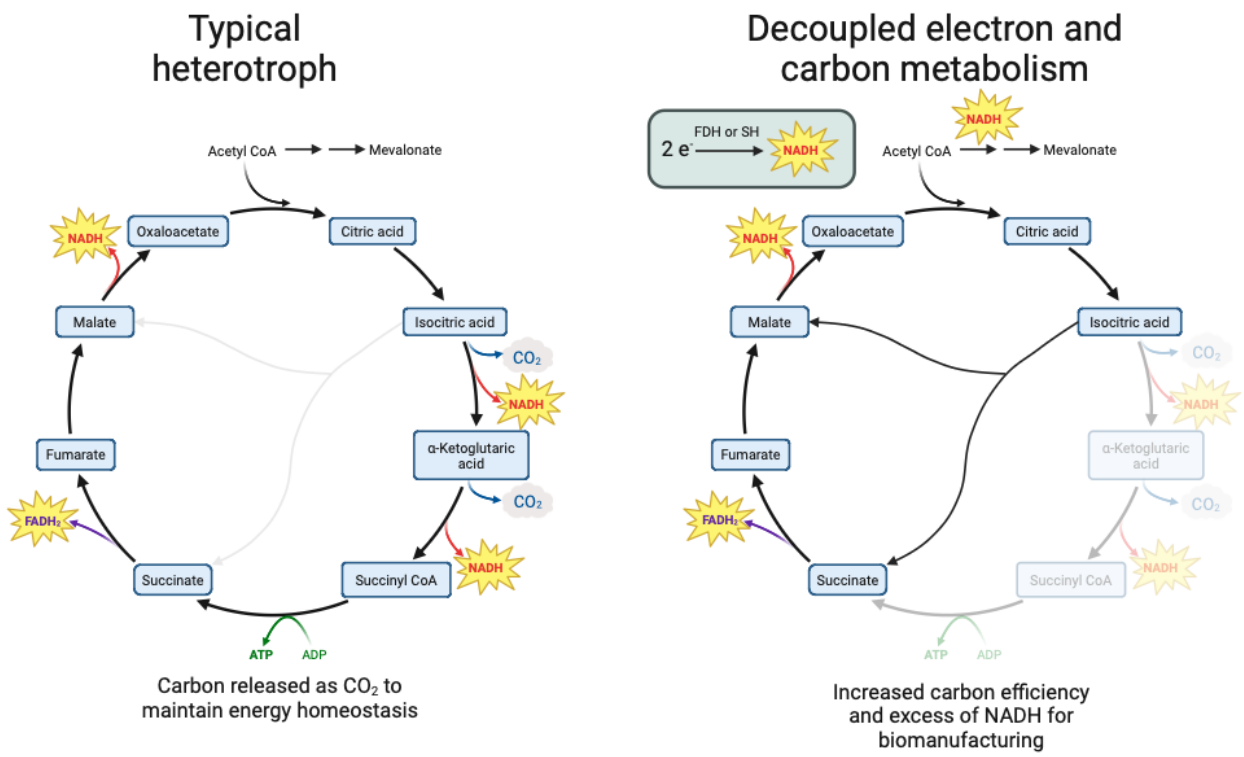

Figure 5. The proposed mechanism for carbon conservation in cells engineered with FDH or HYD is to increase carbon flux through the glyoxylate shunt. Created in BioRender. Panich, J. (2025) https://BioRender.com/l26rpn5

We have observed that cultures treated with H_2 respond by increasing the production of succinate, fumarate, and malate, suggesting activation of glyoxylate shunt metabolism[28,29] (Figure S6 in *SI*). We hypothesize that engagement of the non-oxidative, carbon-retaining glyoxylate shunt pathway could explain how feedstock retention, CO_2 avoidance, and bioproduct formation are possible (Figures 2, 3, 4). Such a metabolism could explain how a microbial host can increase carbon usage efficiency while maintaining redox homeostasis (Figure 5). We note that the magnitude of the increase in mevalonate titer is mild in reversible systems (hydrogenase) and substantial in systems that are essentially irreversible (formate dehydrogenase). While multiple factors may contribute to this outcome, we hypothesize that irreversibility favors carbon flux towards product formation.

Flux balance analysis to evaluate the efficiency of hydrogen gas and formate usage: We used flux balance analysis (FBA) to evaluate the efficiency of hydrogenase and FDH in producing reducing equivalents that would otherwise be derived from oxidizing acetate. FBA is a systems biology technique that utilizes stoichiometric relationships within metabolic networks to compute feasible flux distributions under various constraints without the need for kinetic data. We used FBA to predict the marginal yield envelope of *E. coli,* defined as the range of potential changes in product yield in response to alterations in a specific substrate when supplemented with either hydrogen gas or formate. Typically, FBA operates on an optimization principle, such as

maximizing the molar yield of a product in response to a specific substrate and is based on the assumption that evolution has optimized metabolism to achieve optimal yields. This assumption is valid in model organisms like *E. coli* when cultivated on acetate and glucose, as the observed fluxes and growth rates align with FBA predictions[37]. However, this premise may not hold when using synthetic metabolic pathways, as these pathways are not subject to evolutionary optimization pressures. A limitation of FBA is its presumption that organisms always strive for maximal yield, whereas experiments with *Saccharomyces cerevisiae* and *C. necator indicate* that organisms may also prioritize pathways that sacrifice yield for faster growth rates or metabolic flexibility[38,39]. To validate the computational FBA findings, and as described in the *SI*, we also utilized a heuristic and deductive reasoning approach to estimate molar ratios, where the key step involves equating all energy carriers (ATP, NAD(P)H, $FADH_2$) to proton motive force. As shown in Table 1, the computational FBA and deductive estimates closely align.

Table 1: Compared to untreated *E. coli*, how many moles of hydrogen gas or formate need to be oxidized to…

Metabolic effect*	Hydrogen gas		Formic acid	
	FBA	**Estimate**	**FBA**	**Estimate**
…prevent the complete oxidation of one mole of acetate?	3.40	3.25	2.82	2.89
…enable the formation of one additional gram of dry biomass from glucose?	0.157	0.123	0.131	0.109
…enable the production of one additional mole of mevalonate from glucose via the mevalonate pathway?	15.60	14.75	13.00	13.11
…enable the fermentation of one additional mole of acetate from glucose?	3.60	3.75	3.00	3.33
…enable the fermentation of one additional mole of ethanol from glucose?	6.20	6.25	5.17	5.56
…enable the fermentation of one additional mole of formic acid from glucose?	2.00	1.125	N/A[a]	1.00

[a] Modeling the effects of formic acid addition upon formic acid fermentation resulted in a negative value. *"FBA" is computational flux balance analysis, as described in the main text. "Estimate" uses deductive reasoning to estimate bioenergy requirements based on well-established biochemical facts, as described in SI.

499

500 The efficiency of H_2 or formate in preventing the consumption of acetate (Figures 2 and 3), and
501 of enhancing mevalonate production (Figure 4), can be determined by the following equation:

502 $$Efficiency\ (\%) = \frac{(A_{surplus}\ x\ R_{theoretical})}{(H_{oxidized})} x\ 100$$

503 Where:

504 $A_{surplus}$ = Moles of surplus acetate (Fig. 2B, 3B) or surplus mevalonate (Fig. 4B, 4G)
505 $R_{theoretical}$ = Theoretical moles of H_2 or formate required (Table 1)
506 $H_{oxidized}$ = Moles of H_2 (Fig. S7, 4A) or formate (Fig. S9, 4F) oxidized in culture

507 We have demonstrated a titratable and stoichiometric relationship between H_2 consumption,
508 acetate retention, and CO_2 avoidance (Figure 2; Figure S8 in *SI*). The number of moles of H_2 that
509 are experimentally required to avoid the oxidation of one mole of acetate can be determined by
510 plotting moles of H_2 consumed against moles of acetate retained. The resultant molar ratio is
511 3.925 (± 0.062) (Figure S8B). In contrast, FBA indicates that only 3.40 moles of H_2 are needed
512 (Table 1), suggesting that 86.6% (± 1.8) of the electrons supplied by H_2 were used to replace
513 acetate oxidation as a source of cellular energy. We speculate that the remaining 13.4% of the
514 reducing power was used in off-target reactions not captured by the analysis. Compared to H_2,
515 fewer moles of formate (2.82) are theoretically required to achieve this effect because formate
516 crosses the cell membrane as formic acid, with its proton contributing to the electrochemical
517 potential (Table 1). Similar to H_2, we also performed a formate titration by incrementally increasing
518 formate concentrations and quantifying acetate and CO_2 responses (Figure 3; Figure S8 in *SI*).
519 Plotting the formate consumption and acetate retention data revealed that 2.865 (± 0.102) moles
520 of formate are required to prevent the oxidative decarboxylation of one mole of acetate (Figure
521 S8D), suggesting that 98.4% (± 3.6) of the electrons supplied by formate successfully replaced
522 acetate for cellular energy generation.

523 The efficiency of H_2 or formate in enhancing the formation of mevalonate can be determined in
524 four steps: (1) assess the moles of H_2 or formate oxidized within cultures (Figures 4A, 4F); (2)
525 measure the moles of surplus mevalonate formed within H_2- or formate- treated cultures (Figures
526 4B, 4G); (3) multiply the surplus moles of mevalonate by the number of moles of H_2 or formate
527 that FBA determines is theoretically required to produce this surplus (Table 1); and (4) divide this
528 amount by the total moles of H_2 or formate oxidized within cultures and express the result as a
529 percentage (maximum of 100%). Both H_2 and $HCOO^-$ increased mevalonate biosynthesis
530 (Figures 4B and 4G). Mevalonate is produced by condensing three moles of acetyl-CoA, followed
531 by NADH-dependent reduction. To boost mevalonate formation, electron donors must
532 correspondingly prevent the decarboxylation of three moles of acetyl-CoA and meet this NADH
533 requirement. Analysis of BW-HYD-MEV revealed that of the 181 (± 28) μmol H_2 oxidized by this
534 strain (Figure 4A), only 19.1% (± 8.1) was utilized to enhance mevalonate titer (Figure 4 E).
535 Interestingly, H_2-fed cells had a slightly lower biomass quantity than control cells (Figure 4 C):
536 Compared to control cells, the energy not used for this missing biomass corresponds to the
537 consumption of an additional 58.2 (± 97.7) μmol H_2 by H_2-fed cells (Figure 4E). This shift in cellular
538 energy usage explains how the surplus of mixed acids in H_2-fed cells can require an energy input
539 equivalent to 146.8% (± 26.9) of all H_2 oxidized. The total amount of H_2 theoretically required to
540 facilitate these biochemical changes is thus 120 (± 113) μmol H_2, which is within the error range

of the 181 μmol H_2 experimentally observed as used (See "SUM" in Figure 4E). As compared to H_2, the FBA findings of BW-FDH-MEV were statistically robust: of the 400 μmol formate oxidized, 33.2% (± 7.7) was employed to enhance mevalonate production, 46.9% (± 19.8) was utilized to increase biomass formation, and 8.8% (± 7.4%) was used to boost the production of mixed acid products (Figure 4J). Total biochemical changes relative to water-blanked cultures required the theoretical oxidation of 355 μmol (± 90 μmol) of formate, which aligns with the error of the 400 μmol of formate consumed (See "SUM" in Figure 4J).

Changing the base strain from BW25113 to CM15 resulted in improved mevalonate production efficiency in both CM-HYD-MEV and CM-FDH-MEV. In CM-HYD-MEV, H_2-fed cells now devote 37.8% (± 16.2) of the energy supplied by 70 μmol of oxidized H_2 toward mevalonate formation. However, after considering biomass and mixed acid changes, we were unable to balance total energy requirements between treatment and control conditions (see "SUM" in Figure 4E), a result likely arising from low statistical resolution caused by low H_2 uptake. In contrast to H_2, performance in CM-FDH-MEV was exceptional: virtually all energy provided to CM-FDH-MEV through the oxidation of formate was utilized to enhance mevalonate titer (99.0 ± 2.8%) (see "SUM" in Figure 4J). In conclusion, these data demonstrate that nearly all (within error) of the energy supplied to an industrial host by formate can be harnessed to boost the production of a commodity chemical. However, additional strain engineering will be necessary to improve both the consumption of H_2 and the efficiency of this supplemental energy use.

CONCLUSIONS AND OUTLOOK

Conventional microbial fermentation relies on organic substrates to be metabolized for both energy and product formation. This study moves beyond that paradigm by demonstrating how chemical electron donors can provide an alternative source of cellular energy, eliminating the oxidation of feedstock and allowing their exclusive use for bioproduction. Our findings show that external reducing power can reduce feedstock consumption while avoiding CO_2 production in a stoichiometric manner. Through a series of experiments measuring gas and substrate consumption, we have established that electron donors not only enhance feedstock retention but also increase the efficiency of bioproduct formation. A combined biochemical and computational FBA approach revealed three key insights: (i) electron donors can promote the biosynthesis of a desirable target compound, (ii) metabolic remodeling can increase the proportion of external reducing equivalents directed toward product formation, and (iii) these processes can be efficient. Furthermore, metabolomic analysis suggests that these effects are mediated, at least in part, by the upregulation of glyoxylate shunt metabolism. This provides a unifying hypothesis for CO_2 mitigation and improved carbon utilization, warranting future investigation.

Despite significant advancements, biomanufacturing remains constrained by limited economic feasibility. Can electron donors improve the viability of industrial bioprocesses? While a thorough technoeconomic analysis (TEA) is necessary to fully evaluate this question, our bioenergetic efficiency data provide a basis for exploring its potential. We observed that up to 37.8% of the energy provided to *E. coli through* the oxidation of H_2 can be used to enhance mevalonate formation (Table 1, Figure 4), thereby establishing an experimentally validated benchmark for

efficiency. Glucose, the most widely used biomanufacturing feedstock, has a wholesale price of approximately $0.70 per kg. To compensate for the oxidation of $1.00 worth of glucose would require the expenditure of 283 moles of H_2. Excluding other technoeconomic considerations, if the price of hydrogen gas is $1.77 per kg or lower, a net reduction in operating expenses becomes feasible. If, through future metabolic engineering efforts, the efficiency of H_2 reaches 100% (similar to the 99.0 ± 2.8% efficiency of formate; Table 1, Figure 4), then only 107 moles of H_2 would be necessary, raising price parity to $4.67 per kg.

Notably, the cost of electrolytic H_2 is primarily determined by electricity prices[40,41], and as global energy capacity expands, the levelized cost of electricity from alternative sources is projected to decline by 50% by mid-century[42,43]. It is noteworthy that the price of non-renewable H_2 is already below $1.00/kg. These trends suggest that electron donors could serve as an economically viable alternative energy source, reducing reliance on feedstock-derived energy while enhancing bioprocess efficiency. Conceptually, external reducing power replaces the reducing power ordinarily provided through the oxidation of feedstock, enabling greater bioreactor productivity per unit cost of raw materials. While we demonstrated this principle using mevalonate biosynthesis, the approach is theoretically applicable to any conceivable bioproduct. To realize this vision, our mevalonate assays and flux balance analyses indicate the need for further study of the mechanisms regulating H_2 uptake, as well as how supplemental energy can be redirected toward a desirable metabolic use. We have demonstrated using formate-fed cells that chemical electron donors can be exceptionally efficient at aiding substrate conservation (98.4 ± 3.6% for acetate; Table 1, Figure 3) and product enhancement (99.0 ± 2.8% for mevalonate; Table 1, Figure 4), providing an optimistic benchmark for future biomanufacturing studies.

The development of new technologies in transportation and manufacturing is crucial for energy security and economic growth. Enhancing bioreactor efficiency through cost-effective energy carriers such as H_2 and formate ($HCOO^-$) could play a key role in expanding global biomanufacturing capacity. This strategy complements existing approaches, including the use of lignocellulosic biomass and gaseous waste streams. The engineered strains described herein not only enable carbon-efficient bioproduction but also contribute to a broader framework for the maturing biomanufacturing industry. By simultaneously facilitating CO_2 mitigation and improving substrate conversion yields, these advancements could help accelerate the transition toward a more mature and economically viable bioeconomy.

ACKNOWLEDGEMENTS

This work was funded by the Advanced Research Projects Agency-Energy (ARPA-E: *A Microbial Consortium Enabling Complete Feedstock Conversion*) and by the US Department of Energy (DOE) Joint BioEnergy Institute (https://www.jbei.org), supported by DOE, Office of Science, Biological and Environmental Research Program, under contract DEAC02-05CH11231 between DOE and Lawrence Berkeley National Laboratory. RLB acknowledges funding from the Natural Sciences and Engineering Research Council of Canada (NSERC: 532495-2019). JBR

acknowledges support from a fellowship award under contract FA9550-21-F-0003 through the National Defense Science and Engineering Graduate (NDSEG) Fellowship Program, sponsored by the Air Force Research Laboratory (AFRL), the Office of Naval Research (ONR), and the Army Research Office (ARO). We thank Frank Sergeant (Newcastle University, United Kingdom) for genetic materials and Patrick Hallenbeck† (Université de Montréal, Canada) for advice. The United States Government retains, and the publisher, by accepting the article for publication, acknowledges that the United States Government retains a nonexclusive, paid-up, irrevocable, worldwide license to publish or reproduce the published form of this manuscript, or allow others to do so, for United States Government purposes. Any subjective views or opinions that might be expressed in the paper do not necessarily represent the views of the U.S. Department of Energy or the United States Government.

CONFLICT OF INTEREST STATEMENT

RLB declares a financial interest in Redoxify. JBR declares a financial interest in AlkaLi Labs. JDK declares a financial interest in Ansa Biotechnologies, Apertor Pharma, Berkeley Yeast, BioMia, Cyklos Materials, Demetrix, Lygos, Napigen, ResVita Bio, and Zero Acre Farms. All other authors declare no competing interests.

AVAILABILITY OF SUPPORTING INFORMATION

Primers, plasmids, strains, supporting figures, and supporting tables are available in the accompanying *Supporting Information* file [LINK].

AVAILABILITY OF GENETIC MATERIALS

Primers, plasmids, and strains are listed in Table S1-S3 of *SI* and are freely available for academic use via our institution's Inventory of Composable Elements (ICE)[44]. Please refer to the requisition numbers provided in the *SI*. Please inquire with our institution's Intellectual Property Office regarding commercial use.

References

1. Cowan, A. E., Klass, S. H., Winegar, P. H. & Keasling, J. D. Microbial Production of Fuels, Commodity Chemicals, and Materials from Sustainable Sources of Carbon and Energy. *Current Opinion in Systems Biology* 100482 (2023) doi:10.1016/j.coisb.2023.100482.

663 2. Zhang, Y.-H. P., Sun, J. & Ma, Y. Biomanufacturing: history and perspective. *J. Ind.*
664 *Microbiol. Biotechnol.* **44**, 773–784 (2017).

665 3. Keasling, J. *et al.* Microbial production of advanced biofuels. *Nat. Rev. Microbiol.* **19**,
666 701–715 (2021).

667 4. Levi, P. G. & Cullen, J. M. Mapping global flows of chemicals: from fossil fuel feedstocks
668 to chemical products. *Environ. Sci. Technol.* **52**, 1725–1734 (2018).

669 5. Ng, C. Y., Farasat, I., Maranas, C. D. & Salis, H. M. Rational design of a synthetic
670 Entner-Doudoroff pathway for improved and controllable NADPH regeneration. *Metab.*
671 *Eng.* **29**, 86–96 (2015).

672 6. Tashiro, Y., Desai, S. H. & Atsumi, S. Two-dimensional isobutyl acetate production
673 pathways to improve carbon yield. *Nat. Commun.* **6**, 7488 (2015).

674 7. Meadows, A. L. *et al.* Rewriting yeast central carbon metabolism for industrial isoprenoid
675 production. *Nature* **537**, 694–697 (2016).

676 8. Cui, J. *et al.* Metabolomics Revealed an Association of Metabolite Changes and
677 Defective Growth in Methylobacterium extorquens AM1 Overexpressing ecm during
678 Growth on Methanol. *PLoS ONE* **11**, e0154043 (2016).

679 9. Kang, A. *et al.* Isopentenyl diphosphate (IPP)-bypass mevalonate pathways for
680 isopentenol production. *Metab. Eng.* **34**, 25–35 (2016).

681 10. Lin, P. P. *et al.* Construction and evolution of an Escherichia coli strain relying on
682 nonoxidative glycolysis for sugar catabolism. *Proc Natl Acad Sci USA* **115**, 3538–3546
683 (2018).

684 11. Partipilo, M., Claassens, N. J. & Slotboom, D. J. A Hitchhiker's Guide to Supplying
685 Enzymatic Reducing Power into Synthetic Cells. *ACS Synth. Biol.* **12**, 947–962 (2023).

686 12. Claassens, N. J., Sánchez-Andrea, I., Sousa, D. Z. & Bar-Even, A. Towards sustainable
687 feedstocks: A guide to electron donors for microbial carbon fixation. *Curr. Opin.*
688 *Biotechnol.* **50**, 195–205 (2018).

689 13. Yishai, O., Lindner, S. N., Gonzalez de la Cruz, J., Tenenboim, H. & Bar-Even, A. The
690 formate bio-economy. *Curr. Opin. Chem. Biol.* **35**, 1–9 (2016).

691 14. Cotton, C. A., Claassens, N. J., Benito-Vaquerizo, S. & Bar-Even, A. Renewable
692 methanol and formate as microbial feedstocks. *Curr. Opin. Biotechnol.* **62**, 168–180
693 (2020).

694 15. Sauer, U. *et al.* Metabolic flux ratio analysis of genetic and environmental modulations of
695 Escherichia coli central carbon metabolism. *J. Bacteriol.* **181**, 6679–6688 (1999).

696 16. Lupacchini, S. *et al.* Rewiring cyanobacterial photosynthesis by the implementation of an
697 oxygen-tolerant hydrogenase. *Metab. Eng.* **68**, 199–209 (2021).

698 17. Lubitz, W., Ogata, H., Rüdiger, O. & Reijerse, E. Hydrogenases. *Chem. Rev.* **114**, 4081–
699 4148 (2014).

700 18. Lu, Y. & Koo, J. O2 sensitivity and H2 production activity of hydrogenases-A review.
701 *Biotechnol. Bioeng.* **116**, 3124–3135 (2019).

702 19. Pandelia, M.-E. *et al.* Electronic structure of the unique [4Fe-3S] cluster in O2-tolerant
703 hydrogenases characterized by 57Fe Mossbauer and EPR spectroscopy. *Proc Natl Acad*
704 *Sci USA* **110**, 483–488 (2013).

705 20. Panich, J., Fong, B. & Singer, S. W. Metabolic Engineering of Cupriavidus necator H16
706 for Sustainable Biofuels from CO2. *Trends Biotechnol.* **39**, 412–424 (2021).

707 21. Panich, J. *et al.* Functional plasticity of HCO3- uptake and CO2 fixation in Cupriavidus
708 necator H16. *Bioresour. Technol.* **410**, 131214 (2024).

709 22. Ghosh, D., Bisaillon, A. & Hallenbeck, P. C. Increasing the metabolic capacity of
710 Escherichia coli for hydrogen production through heterologous expression of the
711 Ralstonia eutropha SH operon. *Biotechnol. Biofuels* **6**, 122 (2013).

712 23. Lonsdale, T. H. *et al.* H2-driven biotransformation of n-octane to 1-octanol by a
713 recombinant Pseudomonas putida strain co-synthesizing an O2-tolerant hydrogenase
714 and a P450 monooxygenase. *Chem. Commun.* **51**, 16173–16175 (2015).

715 24. Fan, Q. *et al.* High-Yield Production of Catalytically Active Regulatory [NiFe]-
716 Hydrogenase From Cupriavidus necator in Escherichia coli. *Front. Microbiol.* **13**, 894375
717 (2022).

718 25. Teramoto, H., Shimizu, T., Suda, M. & Inui, M. Hydrogen production based on the
719 heterologous expression of NAD+-reducing [NiFe]-hydrogenase from Cupriavidus
720 necator in different genetic backgrounds of Escherichia coli strains. *Int. J. Hydrogen*
721 *Energy* **47**, 22010–22021 (2022).

722 26. Lamont, C. M. & Sargent, F. Design and characterisation of synthetic operons for
723 biohydrogen technology. *Arch. Microbiol.* **199**, 495–503 (2017).

724 27. Schiffels, J. *et al.* An innovative cloning platform enables large-scale production and
725 maturation of an oxygen-tolerant [NiFe]-hydrogenase from Cupriavidus necator in
726 Escherichia coli. *PLoS ONE* **8**, e68812 (2013).

727 28. Dolan, S. K. & Welch, M. The glyoxylate shunt, 60 years on. *Annu. Rev. Microbiol.* **72**,
728 309–330 (2018).

729 29. Yang, P., Liu, W., Chen, Y. & Gong, A.-D. Engineering the glyoxylate cycle for chemical
730 bioproduction. *Front. Bioeng. Biotechnol.* **10**, 1066651 (2022).

731 30. Schlesier, M. & Friedrich, B. In vivo inactivation of soluble hydrogenase of Alcaligenes
732 eutrophus. *Arch. Microbiol.* **129**, 150–153 (1981).

733 31. Wenk, S. *et al.* An “energy-auxotroph” Escherichia coli provides an in vivo platform for
734 assessing NADH regeneration systems. *Biotechnol. Bioeng.* **117**, 3422–3434 (2020).

735 32. Tishkov, V. I., Galkin, A. G., Marchenko, G. N., Tsygankov, Y. D. & Egorov, A. M.
736 Formate dehydrogenase from methylotrophic bacterium Pseudomonas sp. 101: gene
737 cloning and expression in Escherichia coli. *Biotechnol. Appl. Biochem.* **18**, 201–207
738 (1993).

739 33. Gleizer, S. *et al.* Conversion of Escherichia coli to Generate All Biomass Carbon from
740 CO2. *Cell* **179**, 1255-1263.e12 (2019).

741 34. Jeung, K., Kim, S., Yeon Lee, J. & Yeol Jung, G. Optimization of mevalonate production
742 using acetate by precursor balancing and flux redistribution in Escherichia coli. *Journal of*
743 *Industrial and Engineering Chemistry* (2023) doi:10.1016/j.jiec.2022.12.049.

744 35. Maeda, T., Vardar, G., Self, W. T. & Wood, T. K. Inhibition of hydrogen uptake in
745 *Escherichia coli* by expressing the hydrogenase from the cyanobacterium *Synechocystis*
746 sp. PCC 6803. *BMC Biotechnol.* **7**, 25 (2007).

747 36. Mehrer, C. R., Incha, M. R., Politz, M. C. & Pfleger, B. F. Anaerobic production of
748 medium-chain fatty alcohols via a β-reduction pathway. *Metab. Eng.* **48**, 63–71 (2018).

749 37. Varma, A. & Palsson, B. O. Stoichiometric flux balance models quantitatively predict
750 growth and metabolic by-product secretion in wild-type Escherichia coli W3110. *Appl.*
751 *Environ. Microbiol.* **60**, 3724–3731 (1994).

752 38. Schuster, S., Pfeiffer, T. & Fell, D. A. Is maximization of molar yield in metabolic
753 networks favoured by evolution? *J. Theor. Biol.* **252**, 497–504 (2008).

754 39. Jahn, M. *et al.* Protein allocation and utilization in the versatile chemolithoautotroph
755 Cupriavidus necator. *eLife* **10**, (2021).

756 40. Janssen, J. L. L. C. C., Weeda, M., Detz, R. J. & van der Zwaan, B. Country-specific
757 cost projections for renewable hydrogen production through off-grid electricity systems.
758 *Appl. Energy* **309**, 118398 (2022).

759 41. De Luna, P. *et al.* What would it take for renewably powered electrosynthesis to displace
760 petrochemical processes? *Science* **364**, (2019).

761 42. Sens, L., Neuling, U. & Kaltschmitt, M. Capital expenditure and levelized cost of
762 electricity of photovoltaic plants and wind turbines – Development by 2050. *Renew.*
763 *Energy* **185**, 525–537 (2022).

764 43. Jayadev, G., Leibowicz, B. D. & Kutanoglu, E. U.S. electricity infrastructure of the future:
765 Generation and transmission pathways through 2050. *Appl. Energy* **260**, 114267 (2020).

766 44. Ham, T. S. *et al.* Design, implementation and practice of JBEI-ICE: an open source
767 biological part registry platform and tools. *Nucleic Acids Res.* **40**, e141 (2012).